HHS Public Access

Author manuscript

Cancer Res. Author manuscript; available in PMC 2018 December 15.

Published in final edited form as:

Cancer Res. 2017 December 15; 77(24): 6950–6962. doi:10.1158/0008-5472.CAN-17-0981.

Blocking myristoylation of Src inhibits its kinase activity and suppresses prostate cancer progression

Sungjin Kim[*,1], **Omar Awad Alsaidan**[*,1], **Octavia Goodwin**[1], **Qianjin Li**[1], **Essilvo Sulejmani**[1], **Zhen Han**[1], **Aiping Bai**[2], **Thomas Albers**[3], **Zanna Beharry**[4], **Y. George Zheng**[1], **James S. Norris**[5], **Zdzislaw M. Szulc**[2], **Alicja Bielawska**[2], **Iryna Lebedyeva**[3], **Scott D. Pegan**[1], and **Houjian Cai**[1]

[1]Department of Pharmaceutical and Biomedical Sciences, College of Pharmacy, University of Georgia Athens, Athens, Georgia 30602

[2]Department of Biochemistry and Molecular Biology, Medical University of South Carolina, Charleston, South Carolina 29425

[3]Department of Chemistry and Physics, Augusta University, Augusta, Georgia 30912

[4]Department of Chemistry and Physics, Florida Gulf Coast University, Fort Myers, Florida 33965

[5]Department of Microbiology and Immunology, Medical University of South Carolina, Charleston, South Carolina 29425

Abstract

Protein N-myristoylation enables localization to membranes and helps maintain protein conformation and function. N-myristoyltransferases (NMT) catalyze co- or post-translational myristoylation of Src family kinases and other oncogenic proteins, thereby regulating their function. In this study, we provide genetic and pharmacological evidence that inhibiting the N-myristoyltransferase NMT1 suppresses cell cycle progression, proliferation and malignant growth of prostate cancer cells. Loss of myristoylation abolished the tumorigenic potential of Src and its synergy with androgen receptor in mediating tumor invasion. We identified the myristoyl-CoA analog B13 as a small molecule inhibitor of NMT1 enzymatic activity. B13 exposure blocked Src myristoylation and Src localizaiton to the cytoplasmic membrane, attenuating Src-mediated oncogenic signaling. B13 exerted its antiinvasive and antitumor effects against prostate cancer cells with minimal toxic side-effects in vivo. Structural optimization based on structure-activity relationships enabled the chemical synthesis of LCL204 with enhanced inhibitory potency against NMT1. Collectively, our results offer a preclincal proof of concept for the use of protein myristoylation inhibitors as a strategy to block prostate cancer progression.

Keywords

Myristoylation; NMT; Src family kinases; B13; prostate tumorigenesis

Correspondence to: Houjian Cai, Ph.D, Department of Pharmaceutical and Biomedical Sciences, Room 418, Pharmacy South, College of Pharmacy, University of Georgia, Athens, Athens, GA 30602, Office: 706-542-1079, FAX: 706-542-5358, caihj@uga.edu.
[*]Co-first author

The authors disclose no potential conflicts of interest.

Introduction

N-myristoylation is a co/post-translational modification that results in the covalent attachment of the 14-carbon saturated myristic acid to the N-terminus of a target protein (1). N-myristoyltransferase (NMT) catalyzes this transfer of the myristoyl- group of myristoyl-CoA to a glycine in the N-terminus. N-myristoylation is ubiquitously found in eukaryotes, and two mammalian NMT isoforms, NMT1 and NMT2, have been identified that share 77% identity (2). NMTs have been considered as promising targets for the development of antifungal, antiparasitic, and antitumor progression therapeutics (3).

One set of proteins where myristoylation has been observed to play an important role is Src family kinases (SFKs). Myristoylation together with other modifications allow SFKs to attach to the cytoplasmic membrane and mediate their kinase activity and cellular functions (4, 5). SFKs are pleiotropic activators in signal transduction pathways and numerous studies have documented their role as oncogenic driver genes in a variety of cancers (6). SFKs interact with a variety of cellular receptors, and are downstream effectors of G protein-coupled receptors, integrins, and many receptor tyrosine kinases (RTKs) (7, 8). Activation of SFKs also activates a variety of downstream signaling to facilitate tumor growth, angiogenesis, and metastatic invasion (6, 9, 10). Particularly, aberrant expression of Src kinase facilitates the phosphorylation of androgen receptor (AR) and bypasses ligand dependent AR activation in castration resistant prostate cancer (9, 11). Our previous study showed that co-overexpression of Src and AR promotes invasive prostate adenocarcinoma (11, 12).

In vitro studies have indicated that NMT1 regulates Src kinase myristoylation and phosphorylation or kinase activity in COS-1 cells (5) or HT-29 cells (13). Here we further study if genetic and pharmacological inhibitions of NMT1 regulate proliferation of prostate cancer cells and growth of prostate tumor *in vivo*. We demonstrate that knockdown of NMT1 suppressed proliferation of prostate cancer cells by blocking cell cycle progression, and inhibited the myristoylation and tyrosine phosphorylation of Src kinase. The inhibitory effect increased with increasing expression levels of NMT1. Myristoylation was shown to facilitate SFKs-mediated prostate tumorigenesis, and mediate the interaction of Src kinase with AR, with the synergistic effect of promoting prostate tumor progression. Screening a panel of small molecule compounds based on the myristoyl-CoA scaffold identified a compound that blocked the enzymatic activity of NMT1 and myristoylation of Src kinase. The inhibitor suppressed proliferation, migration and invasion of prostate cancer cells and tumor growth with a limited toxicity to normal cells or major organs *in vivo*. The inhibitory activity of this compound was optimized through structurally guided and SAR based methods. Our study provides a novel therapeutic approach for the treatment of prostate cancer by targeting lipidation.

Materials and Methods

Plasmid constructs

The open reading frames of the Src(WT) and its mutants [(Src(WT/G2A), Src(Y529F), Src(Y529F/G2A), Src(Y529F/S3C/S6C), Src(Y529F/G2A/S3C/S6C), Src(Y529F/K298M)], Fyn(WT) and its mutants [(Fyn(WT/G2A), Fyn(Y528F), Fyn(Y528F/G2A), Fyn(Y528F/C3S/C6S), Fyn(Y528F/G2A/C3S/C6S), Fyn(Y528F/K298M)], and AR genes were cloned into FUCRW or FUCGW lentiviral vectors as described previously (14, 15). Src(Y529F) and Src(Y529F/G2A) were also cloned into the pTK380 vector (16), designated as TRE/Src(Y529F), which expresses the reverse tetracycline-controlled transactivator (rtTA), and is regulated by doxycycline (Dox). To knock down the human Src and NMT1 genes, shRNAs targeting Src and NMT1 were generated using primers listed in Table S1. After the primers were annealed, the inserts were cloned into psiRNA-W [H1.4] vector at the Bbs I site. The shRNAs with the H1 promoter were further sub-cloned into FUCRW and/or FUCGW lentiviral vectors at the Pac I site. To knock down the human Fyn gene, shRNA constructs were purchased from Sigma.

Cell culture

PNT2 cells were purchased from Sigma (Cat#95012613). 293T and prostate cancer cell lines including LNCaP, 22Rv1 DU145, and PC-3 were purchased from American Type Culture Collection (ATCC). The above cell lines were obtained in September 2013 and were defined as passage 1 (the first thawing) when arrived in the lab. SYF1 ($Src^{-/-}Yes^{-/-}Fyn^{-/-}$) mouse fibroblast cell line and LNCaP-abl, and 293T expressing rtTA (293T-rtTA) were gifts from Dr. Jonathan Cooper's lab in August 2008 (17), Dr. Qianben Wang's lab in March 2016 (18), and Dr. Kathrin Plath's lab in May 2008 (12), respectively. Cancer cell lines were cultured in ATCC-recommended medium, and LNCaP-abl was grown in 10% charcoal-stripped fetal calf serum. Cell lines from ATCC and Sigma had a certificate of mycoplasma-free and authentication when purchased. Other cell lines including SYF1 and LNCaP-abl were tested by the universal mycoplasma detection kit (ATCC Cat# 30-1012K) and determined to be mycoplasma free. PNT2, LNCaP, 22Rv1 DU145, and PC-3 lines were used within no more than 8–10 passages. LNCaP-abl cells were at 62 passages in this study. SYF1 cells and 293T-rtTA cells were used at the passage of less than 35. Loss of Src and Fyn expression in SYF cells was confirmed by Western analysis as indicated in each experiment. The doxycycline induction ability in 293T-rtTA did not show any difference in terms of cell passage number. SYF1 cells transduced with Src/Fyn(WT) or their mutants, or 293T-rtTA transduced with TRE/Src(Y529F) by lentiviral infection (12) were grown in DMEM with 10% FBS (HyClone, Logan, UT). The expression of Src kinase was induced by 1 μg/mL doxycycline. All the cell lines were periodically examined for mycoplasma contamination.

Protein fractionation

The fractionation protocol for the cytosol and the cytoplasmic membrane were as described previously with slight modification (19). Briefly, SYF1 cells expressing Src/Fyn(WT) or its mutants were incubated in DMEM including 2% bovine serum albumin (BSA) for 24 h. After lysing with TNE lysis buffer (50 mM Tris, 150 mM NaCl, 2 mM EDTA pH 7.4,

protease inhibitor cocktail, and phosphatase inhibitor cocktails), the protein extracts were homogenized using a 25-gauge needle syringe (15 strokes) and centrifuged at 14,000 rpm for 10 min. The supernatant was collected as the cytosolic (Cyt.) fraction. Pellets were rinsed twice with TNE lysis buffer and re-suspended in TNE lysis buffer which contained 60 mM β-octylglucoside. Samples were incubated on ice for 30 min and centrifuged at 14,000 rpm for 20 min at 4°C. The supernatants were collected as the total membrane (TM) fraction.

Crystallization of NMT1 and structure determination

Purified NMT1 was dialyzed overnight against a buffer containing 20 mM Tris pH 7.5, 100 mM NaCl, and 1 mM DTT. The enzyme was concentrated to 6.3 mg/mL and incubated at a 1:5 molar ratio with myristoyl CoA. This mixture was filtered with a 0.2 μm filter. NMT1 crystals were obtained through vapor drop diffusion using a 500 μL reservoir with a 4 μL hanging drop containing equal parts of NMT1 and reservoir solution (22.5% PEG 4000, 5 mM $NiCl_2$, 100 mM sodium citrate pH 4.5, and 2.5% glycerol) (20). The crystals were flash frozen in liquid nitrogen using the reservoir solution as a cryoprotectant. The data was collected at the SER-CAT 22ID beamline at 1 Å using a MAR300hs detector. HKL-2000 was used to index, integrate, and scale data sets. Phenix and coot were used for molecular replacement and refinement of the structure.

Detecting the myristoylation of Src kinase by Click chemistry

To evaluate myristoylation of proteins, PNT2, LNCaP, LNCaP-abl, 22Rv1, PC-3, and DU145 cancer cells were grown in the ATCC-recommended medium with myristic acid azide. The protein lysates were extracted using M-PER buffer, and a 40 μL protein lysate aliquot was used for the Click reaction. Myristoyl-proteins were detected by immunoblotting using Streptavidin-HRP.

To detect the effect of NMT1 on expression levels of myristoylated Src protein, PC-3 cells were transduced with shRNA-control or shNMT1. Additionally, to examine the inhibition of B13 on Src myristoylation, PC-3 cells were treated with 0, 1, 15, 30 μM of B13 for 2 h. The shNMT1 transduced or B13-treated cells were cultured in the medium with 60 μM of myristic acid-azide for 24 h. Proteins were extracted with M-PER buffer (Thermo Scientific) containing protease inhibitors and phosphatase inhibitors. Cell lysates were centrifuged at 14,000 rpm for 20 min. The supernatants were incubated with Src antibody for 16 h at 4°C. Protein A agarose beads were added, and the mixtures were incubated for 1 h at 4°C. After washing five times with IP lysis buffer, the Click chemistry reaction was accomplished by adding Click reagents according to the manufacturer's instructions (Life Technologies). In brief, 30 μL of the Click-iT reaction buffer containing 40 μM alkyne-biotin, 10 μL of $CuSO_4$, and 10 μL of additive 1 solution was mixed with the equal volume of immunoprecipitated agarose beads. Then 20 μL of additive 2 solution was added. The myristoyl-Src was further mixed with loading buffer and boiled. The lysate was detected by immunoblotting using Streptavidin-HRP.

To screen the compounds inhibiting the Src myristoylation, SYF1($Src^{-/-}Fyn^{-/-}Yes^{-/-}$) cells were transduced with Src(WT) or Src(G2A) by lentiviral infection. The transduced cells

were grown in DMEM with 2% fatty acid free BSA containing 60 μM myristic acid-azide for 24 h after pre-treatment of LCL or GRU compounds for 2 h. To examine Src myristoylation in a dose dependent manner, SYF1+Src(WT) cells were treated at 0, 1, 5, 15, 30 μM of B13 for 2 h, followed by the addition of 60 μM of myristic acid azide. The expression levels of myristoyl-Src (60 kDa) were detected by immunoblotting.

Screening for NMT1 inhibitors and measurement of IC_{50}

For screening of NMT1 inhibitors or the measurement of IC_{50}, the 1× reaction buffer (50 mM HEPES and 0.5 mM EDTA), 140 nM of NMT1 purified enzyme (See the NMT1 purification Section, the enzyme stock was preserved in the buffer containing 1mM EDTA, 250 mM NaCl, and 20 mM Tris pH 8.5), 5 μM of peptide Gly-Ser-Asn-Lys-Ser-Lys-Pro-Lys (derived from the N-terminus of human pp60Src tyrosine kinase), and the inhibitor at 0, 10, 20, 40, 80, 120, 160, or 200 μM respectively were mixed in a 96-well plate. After incubation at 30 °C for 10 min, the reaction was started by adding 1 μM myristoyl coenzyme A (Avanti Polar Lipids). The total volume of the above mixture was set 80 μL/well. After incubation at 30 °C for 60 min, the released coenzyme A was detected by adding 80 μL of 30 μM of 7-diethylamino-3-(4'-maleimidylphenyl)-4-methylcoumarin (CPM) stock solution (Sigma Aldrich) to each well and incubated in the dark for 12 min. The fluorescence intensity was measured by a Flex Station 3, microplate reader (excitation at 390 nm; emission at 479 nm).

Analysis of mRNA copy number in TCGA database

Expression values were extracted from the cBioPortal for Cancer Genomics (http://www.cbioportal.org/) for the following genes using the Gene Set Query functions: NMT1 and Src. The expression values were then cross-referenced with the data sets from the TCGA Data Portal. The data was then downloaded and aligned to the respective TCGA Sample IDs in order to be used in statistical analysis. Additional data was extracted from the TCGA Provisional Prostate Adenocarcinoma clinical data set (http://www.cbioportal.org/study?id=prad_tcga#clinical), giving more information for each Sample ID such as: Gleason Score, Survival Status, Days to Sample Collection, and Cancer status.

Soft agar colony formation assay

The effect of Src(WT), Src(Y529F), Src(Y529F/G2A), Src(Y529F/S3C/S6C), and Src(Y529F/K298M) on colony formation in SYF1 cells was assessed by soft agar colony formation assay using Cell Transformation Detection Assay Kit (Millipore, Darmstadt, Germany). The assay was performed in six-well plates as follows: 1 mL of 0.8 % agar solution was layered in the bottom of each well followed by 0.5 mL of 0.4 % agar solution as the top layer. A total of 1,500 cells were suspended in 0.4 % top layer agar containing 0.5 mL of DMEM with 10% FBS and plated on top of the bottom layer in the same medium according to the manufacturer's instructions. After 21–28 days of incubation at 37°C in a 5% CO_2 incubator humidified atmosphere, the number of colonies were counted and photographed under a fluorescence microscope (Carl Zeiss, Germany).

Cell proliferation, invasion, migration assay, and cell cycle analysis

For cell proliferation assays, cells were seeded in 96-well plates at a density of 3000–5000 cells per well and treated with different concentrations of B13. The medium was removed and replaced with 100 μL of fresh culture medium without phenol red. Next, 10 μL of 12 mM MTT (ThermoFisher) was added to each well, and incubated at 37 °C for 4 h. The reaction was stopped using 100 μL of 10% SDS (dissolved in 0.01 M HCl), and incubated at 37 °C for another 4 h. The absorbance was measured at 570 nm (FlexStation 3, Molecular Devices).

For wound-healing assays, 8×10^5 cells were seeded in a 6-well plate and incubated for 24 h. Once the cells reached 95% confluence, a space was created using a 1 mL pipette tip to scratch wounds across the well. After washing with medium to remove floating cells, fresh medium with a tested compound was added. The scratched space was monitored and imaged daily.

For cell migration assays, cells were cultured to around 80% confluence. After incubation for 24 h in serum free medium, the cells were seeded according to the manufacturer's instructions. The top well contained medium with compound or DMSO, and the receiver well contained 10% FBS. After 48 h incubation, the medium was removed from the insert and washed with PBS, then fixed with 3.7% formaldehyde for 2 min and methanol for 20 min. The fixed cells were washed with PBS, and stained with 0.1% crystal violet at room temperature for 15 min in the dark. After washing with PBS, the non-migrated cells were removed with cotton swabs, and the migrated cells were imaged and counted.

For cell cycle analysis, cells were grown in ATCC-recommended medium. After attaching, the medium was replaced with fresh medium with/without 15 or 30 μM of B13 every 24 h for 3 days. 1×10^6 cells were obtained from the plate, and washed with PBS, then fixed with 70% ethanol for 1 h at 4 °C. After washing with PBS, the fixed cells were stained by FxCycle™ propidium iodide/RNAse solution (Invitrogen) for 30 minutes in the dark at room temperature. The stained cells were then analyzed by flow cytometry (CyAn ADP Analyzer, 488 nm excitation and 585nm emission).

Prostate regeneration assay and xenograft tumors

C57BL/6J and CB.17$^{SCID/SCID}$ (SCID) mice were purchased from Taconic (Hudson, NY). For the prostate regeneration assay, primary prostate cells were isolated from 8–12 week-old male C57BL/6J mice, and infected with lentivirus expressing Src/Fyn(WT) or mutants, or co-infected with Src(WT)/Src(G2A) and AR according to the experimental setup. Infected cells ($2–3 \times 10^5$ cells/graft) were combined with urogenital sinus mesenchyme (UGSM) ($2–3 \times 10^5$ cells/graft) together with 25 μL of collagen type I (adjusted to pH 7.0) (12). After overnight incubation, grafts were implanted under the kidney capsule in SCID mice by survival surgery. All animals were sacrificed at 8 weeks after grafts were implanted.

To examine the role of Src or NMT1 in tumor progression, the xenograft tumor model was applied. PC-3 cancer cells transduced with Src-shRNA, NMT1-shRNA or control shRNA by lentiviral infection and were grown in DMEM with 10% FBS. 3×10^5 cells were mixed with 50 μL of collagen type I (pH 7.0) (BD Biosciences) and inoculated subcutaneously in both

lateral flank sides of SCID mice. The size of tumors was measured weekly. The host mice were sacrificed, and xenograft tumors were harvested after two months incubation.

For examining the inhibition of B13 on xenograft tumors, PC-3 cells were subcutaneously inoculated in the flank side of SCID mice. Mice carrying xenografts were randomly separated into two groups after 2–3 weeks. B13 was dissolved in the vehicle solution containing 30% kolliphor, 65% saline (0.9% NaCl), and 5% ethanol. Mice were administrated intravenously (i.v) with 200 μL of the drug solution at a concentration of 75 mg/kg body weight or vehicle twice a week for 4–6 weeks. Body weight and tumor size were measured (length × width) weekly. Xenograft tumors, the liver, lung and kidney were harvested for immunohistochemistry analysis. All animals were maintained according to the surgical and experimental procedures of the protocol A2013 03-008 approved by IACUC at the University of Georgia.

Statistical Analysis—Prism software was used to carry out statistical analyses. The data are presented as mean ± SEM and analyzed using the Student's t test. All t tests were performed at the two-sided 0.05 level for significance. "*": $P<0.05$; "**":$P<0.01$; "N.S.": not significant.

RESULTS

Ablation of N-myristoyltransferase 1 inhibits proliferation of prostate cancer cells

Protein lipidation including myristoylation is essential for regulation of the structure and function in numerous disease-related proteins (3). N-myristoyltransferase (NMT) catalyzes protein myristoylation, and has been considered a major target to block cancer progression (13, 21). NMT1 was expressed in normal or prostate cancer cells, and mRNA and protein expression levels of NMT1 were significantly elevated in DU145 and PC3 cancer cells (Fig. 1A–B). Increased expression of NMT1 correlated with elevated protein myristoylation at ~60 kDa (Fig. 1C). To examine if NMT1 regulates the growth of prostate cancer cells, shRNA targeting NMT1 (shNMT1) was generated (Fig. S1A–B). Knockdown efficiency was validated in SYF1 ($Src^{-/-}Yes^{-/-}Fyn^{-/-}$) cells expressing Src(WT) by demonstrating a reduction in myristoylated Src kinase using Click chemistry (Fig. S1C). While knockdown of NMT1 showed no inhibition on the growth of PNT2 cells (normal cells), it inhibited the proliferation of LNCaP, 22Rv1, DU145, and PC-3 prostate cancer cells (Fig. 1D and Fig. S1D). In particular, the inhibitory effect on cell proliferation correlated with the expression levels of NMT1 (Fig. 1E) and the lack of inhibition of normal cells (PNT2 cells) suggests that NMT1 might serve as a potential inhibition target in prostate tumors without causing major toxicity.

PC-3 cells were selected for xenograft studies since NMT1 expression was highest in this cell line. Knockdown of NMT1 significantly inhibited the growth of PC-3 xenograft tumors leading to a decrease in the size and weight of tumors (Fig. 1F–G). Suppression of NMT1 led to cell cycle arrest at the S-phase with a decrease of the cell population at the G2/M phase (Fig. 1H), but had no significant effect on cell apoptosis (Fig. 1I).

NMT1-Src axis mediates proliferation of prostate cancer cells

Myristoylation of Src kinase regulates its kinase activity (5). SFKs are important oncogenic driver genes in a variety of cancers including advanced stages of prostate cancer (9, 22). Expression levels of NMT1 and Src kinase were significantly correlated in human tumors (Fig. 2A) and expression levels of NMT1 correlated with the active Src kinase [detected by pSrc(Y416) antibody] in prostate cancer cells (Fig. 1B). Similar to the effect of shRNA-NMT1 on PC-3 xenografts, the growth of PC-3 cancer cells (Fig. S2A–B) and xenografts (Fig. 2B) were dependent on expression of Src kinase. Knockdown of another SFK member Fyn kinase led to only mild inhibition of PC-3 and LNCaP cell proliferation (Fig. S2C–D). Down-regulation of NMT1 appears to inhibit Src myristoylation (Fig. 2C), tyrosine phosphorylation (pSrcY416), and the level of FAK phosphorylation, a downstream target of Src kinase (Fig. 2D), highlighting a potential NMT1-Src axis to inhibit tumor growth, particularly in Src-driven tumors.

Single and double knockdown of NMT1 and Src were performed to evaluate the effect on cell proliferation in LNCaP, 22Rv1, and PC-3 cell lines. Single knockdown of Src or NMT1 inhibited proliferation of the three cell lines (Fig. 2E) but double knockdown (shSrc and shNMT1) showed no additive effect in LNCaP and 22Rv1 cells. However, double knockdown in PC-3 cells (showing the highest expression of NMT1 and pSrc) showed greater inhibition of proliferation compared to either single knockdown (Fig. 2E). These results demonstrate an NMT1-Src axis that plays a role in prostate cancer cell growth.

Loss of N-myristoylation inhibits SFK-induced oncogenic signaling *in vitro* and prostate tumorigenesis *in vivo*

The tumorigenic potential of the following Src and Fyn kinase mutants were examined *in vitro* and *in vivo*: constitutively active that recapitulates activated Src kinase in tumors [Src(Y529F) or Fyn(Y528F)], loss of the myristoylation site [Src(Y529F/G2A) or Fyn(Y528F/G2A)], gain [Src(Y529F/S3C/S6C)] or loss [Fyn(Y528F/C3S/C6S)] of two palmitoylation sites, and loss of both myristoylation and palmitoylation sites [Fyn(Y528F/C3S/C6S/G2A)] (Fig. 3A and 3B). Src(Y529F/G2A), Fyn(Y528F/G2A) and Fyn(Y528F/C3S/C6S/G2A) inhibited phospho-Erk, pFAK expression (Fig. S3A and B), and colony formation (Fig. S3C and D), suggesting that specifically myristoylation and not palmitoylation is essential for SFKs-mediated oncogenic signaling and transformation *in vitro*.

As previously reported (17), while regenerated tissue derived from Src(Y529F) or Fyn(Y528F/C3S/C6S) infected epithelial cells formed a solid tumor (Fig. 3C–D), tissue from Src(Y529F/S3C/S6C) showed normal tubule structure (Fig. 3C and E). Src(Y529F)-induced tumors were composed of sheets of poorly differentiated carcinoma cells without glandular structures and with focal sarcomatoid areas (Fig. 3C). In contrast, the regenerated tissue derived from Src(Y529F/G2A) showed normal tubule structure (Fig. 3E). Additionally, regenerated prostate tissue derived from Fyn(Y528F) and Fyn(Y528F/C3S/C6S) exhibited high grade adenocarcinoma and invasive tumor, respectively (17). The tissues from Fyn(Y528F/C3S/C6S) showed solid tumors with un-differentiated tumorigenic cells. In contrast, tissues from Fyn(Y528F/G2A) or Fyn(Y528F/C3S/C6S/G2A) showed

normal glandular tubules (Fig. 3D and F). Collectively, these results indicate that myristoylation is essential for SFKs-induced tumorigenesis and loss of myristoylation abolishes tumorigenic potential, suggesting that myristoylation is an important oncogenic target.

Blockade of myristoylation inhibited synergy of Src and AR in prostate tumorigenesis

Co-expression of c-Src and AR induces activation of Src kinase and leads to invasive prostate tumorigenesis *in vivo* (12). The role of myristoylation in the synergy of Src-AR induced tumorigenesis was also examined. Prostate primary cells were transduced with AR, Src(WT), Src(G2A), AR+Src(WT), or AR+Src(G2A) by lentiviral infection (Fig. 4A). Their expression was visualized in the regenerated tissues by fluorescence imaging of the GFP/RFP markers (Fig. 4B). Although the size of regenerated tissue showed no visible difference, the weight of regenerated tissue derived from Src(WT)+AR increased significantly in comparison with Src(WT), Src(G2A), AR, or Src(G2A)+AR (Fig. 4B). As reported previously (12), over-expression of AR or Src(WT) alone did not induce prostate tumorigenesis, and regenerated tissues contained histologically normal prostate tubules (Fig. 4C). Regenerated tissues derived from Src(WT)+AR displayed phenotypic features of a poorly differentiated or undifferentiated high grade carcinoma with an invasion of some tumorigenic cells into the neighboring tissues. While normal tubules usually contains a large lumen cavity, tumors from Src(WT)+AR tumors are comprised of tumorigenic cells without cavity. As a result, although regenerated tissues showed no difference in size, the weight of regenerated tissue from Src(WT)+AR group was significantly elevated than those from normal tubules. In contrast, regenerated tissues derived from over-expression of Src(G2A) alone or Src(G2A)+AR showed normal tubule structure (Fig. 4C), suggesting that loss of Src kinase myristoylation blocks the synergy of Src(WT) and AR induced tumorigenesis *in vivo*. Since myristoylation was important for Fyn transformation, the synergy of AR and Fyn was examined. However, the results showed no synergistic effect in the regenerated tissues (Fig. S4A–B), suggesting differential functions of Src family kinases (17), likely dictated by differential intracellular trafficking pathways (23).

Loss of Src myristoylation interfered with the protein interaction of exogenously expressed Src and endogenous AR in LNCaP (Fig. S5A–C) and 22Rv1 prostate cancer cells (Fig. S5D–F) in the presence or absence of AR agonist (R1881), and inhibited AR-regulated expression of the PSA, KLK2, and TMPRSS2 genes (Fig. S5G). These results further suggest that myristoylation is a potential therapeutic target for the inhibition of Src kinase function and its mediated tumorigenesis.

Small molecule targeting of NMT1 enzymatic activity

To identify small molecule compounds that target NMT activity, recombinant NMT1 protein (with an exclusion of the 108 amino acids DNA sequence in the N-terminus) was used (Fig. S6A–B). The protein was purified by affinity chromatography (Fig. S6C) (20). A fluorescence-based *in vitro* assay was developed (Fig. S7A) (24) and the myristoylation process was found to occur by a “Ping-Pong” mechanism (Fig. S7B). The detection of Src myristoylation using click chemistry was developed to examine the inhibition of compounds at the cellular level (Fig. S8A–B). The assays were used to screen a selected panel of LCL

compounds of previously synthesized myristoyl-CoA analogs (Fig. S8C and Fig. S9). D-NMAPPD, N-[(1R,2R)-2-hydroxy-1-(hydroxymethyl)-2-(4-nitrophenyl)ethyl]-tetradecanamide, also named B13 (or LCL4), was the top hit that inhibited NMT1 activity and Src kinase myristoylation (Fig. 5). The IC_{50} of B13 (77.6 μM) was not improved with analogs with longer or shorter N-acyl carbon chains on R1 group such as LCL7 or LCL35 likely due to steric clashes of the longer tails or loss of hydrophobic interactions with shorter tails with the NMT1 protein (Fig. 5). Additionally, when the nitro (R2 group) was removed from the *p*-position of the aromatic ring of LCL4 along with the addition of hydroxymethyl (R4 group) such as the compound LCL1, it showed a significant increase in IC_{50} value. However, N,N'-Disubstituted urea as a linker between aromatic ring and aliphatic tail such as LCL17 led to a decrease of the IC_{50} value, which could be due to the planar and non-flexible nature of the –NH-CO-NH- linker (Fig. 5).

B13 and its derivative LCL204 compete with the myristoyl-CoA binding site of NMT1

B13 is structurally similar to myristoyl-CoA as both contain a 14-carbon alkyl tail (Fig. 6A). The crystal structure of NMT1 was solved to understand how B13 interacts with NMT1 (Table S2). Similar to the reported structure (20), the myristoyl-CoA binding site of NMT1 was identified in our structure and placement of B13 within this site was performed initially by overlaying B13's alkyl tail with that of myristoyl-CoA (Fig. 6B). Additionally, orientation of B13 within the active site was driven by the SAR data (Fig. 6B and S9). Several favorable interactions between B13 and the NMT1 binding pocket, including the interaction of 1) the aromatic ring with a hydrophobic patch comprised of Tyr180 and Val181; 2) the aliphatic tail with Asn246; 3) potential hydrogen bonds between R2 nitro group and Arg255, between the amide group and Thr282 and the backbone amide of Leu248, and between the R4 hydroxymethyl group and the hydroxyl group of Tyr180 (Fig. 6B).

The interactions of B13 and NMT1 described above were used to identify an analog with improved efficacy. Based on the B13-NMT1 model in Fig. 6B, the hydroxymethyl group and carbonyl oxygen are competing for hydrogen bonding interactions with NMT1. Therefore, the removal of the carbonyl could potentially enhance binding and thus increase inhibition. Molecular modeling by using Autodock Vina further suggested that the carbonyl group behaved in a more rigid manner than the NO_2 moiety (Fig. 6B) and could extend the half-life due to introduction of the stable alkane group. To probe the predictive accuracy of this structural placement and molecular modeling, LCL204 was synthesized (Fig. 6A–B) and found to exhibit an order of magnitude enhancement in potency towards NMT1 (IC_{50} = 8.7 μM, Fig. 6C). These results suggest a likely path forward for further structure optimization for greater potency in targeting NMT1 activity.

B13 inhibits Src myristoylation, localization at the cytoplasmic membrane, and its mediated oncogenic signaling and transformation

Src myristoylation is a down-stream target of NMT1. B13 inhibited Src myristoylation of ectopically expressed Src kinase or endogenous Src kinase (Fig. 6D–E). Myristoylation is essential for the attachment of Src family kinases at the cytoplasmic membrane. The majority of Src/Fyn proteins were found to localize in the cytosol in the Src(G2A),

Src(Y529F/G2A), Fyn(G2A), and Fyn (Y528F/G2A) mutants (Fig. S10A–D). Loss of myristoylation inhibited the association of Src kinase with the cellular membrane (Fig. S10E). B13 inhibited Src kinase tyrosine phosphorylation [detected by pSrc(Y416)] in association with down-regulation of pFAK and pAkt (Fig. 6F), or suppression of *de novo* synthesized Src-induced signaling (Fig. 6G). Similarly, the amount of non-phosphorylated Src kinase in the open conformation [detected by non-pSrc(Y527)] at the cytoplasmic membrane, representing the doxycycline induced *de novo* synthesized Src kinase, was reduced after treatment with B13 (Fig. 6H). Expression levels of non-phosphorylated Src in the cytoplasmic fraction did not change with B13 treatment most likely because only a small portion of the total cytosol lysate was analyzed due to the limited loading volume available in the gel. Additionally, while Src(Y529F) significantly increased colony formation, the transformation was inhibited by B13 (Fig. 6I).

B13 inhibits proliferation, migration, and invasion of prostate cancer cells and growth of xenograft tumors

The ability of B13 to inhibit transformation and proliferation of prostate cancer cells was examined. B13 significantly inhibited proliferation of 22Rv1, PC-3, and DU145 prostate cancer cells, but this effect was less sensitive in LNCaP cells (Fig. 7A), which is correlated with the lower expression of NMT1 (Fig.1A–B). Cell cycle progression was significantly inhibited in the tested prostate cancer cells (Fig. 7B). The cell cycle inhibition was further confirmed by decreased expression of CDK2 and cyclin D1, increased expression of p27 in PC-3 and DU145 cells, and decreased expression of CDK6 in DU145 cells (Fig. 7C). B13 also suppressed invasion of 22Rv1 and migration of PC-3 cancer cells (Fig. 7D). However, B13 had a limited effect on PNT2 normal cell proliferation and did not affect the cell cycle in PNT2 cells (Fig. S11A–C) or proliferation of 293T cells (Fig. S11D).

To examine the specificity of B13 for targeting the NMT1-Src axis, 22Rv1 or PC-3 cells transduced with shRNA-control or shRNA-Src were subjected to the B13 treatment. Single B13 treatment or knockdown of Src showed significant inhibition on proliferation of 22Rv1 and PC-3 cells (Fig. S12A–B). PC-3 cells with Src knockdown and B13 treatment showed a combined effect on reducing proliferation (shRNA-Src+B13 versus B13) (Fig. S12A). This effect on proliferation was not observed in 22Rv1 cells (shRNA-Src+B13 versus shRNA-Src) (Fig. S12B). As PC-3 cells showed the highest and 22Rv1 the lowest expression of NMT1 and pSrc, this data suggests that the NMT1-Src axis sensitizes cells to targeting myristoylation to reduce proliferation.

The effect of B13 in host mice carrying PC-3 xenograft tumors was further examined. B13 significantly inhibited the size and weight of PC-3 xenograft tumors (Fig. 7E) with no observed pathological toxicity to the major organs of host SCID mice including the liver, kidney, and lung (Fig. 7F), and no significant changes in body (Fig. S13A) or organs' weight (Fig. S13B). Collectively, B13 exhibited inhibition on the growth of prostate cancer cells, suggesting its potential as an effective agent for the treatment of prostate tumors.

Discussion

Our study demonstrates that the inhibition of NMT1 genetically or pharmacologically suppresses proliferation of prostate cancer cells and growth of xenograft tumors. The magnitude of the inhibitory effect is positively correlated with the expression levels of NMT1 and pSrc(Y416) in cancer cells. Inhibition of NMT1 suppresses myristoylation and tyrosine phosphorylation of Src kinase *in vitro* and *in vivo*. Targeting myristoylation exhibits dual effects in inhibiting Src-mediated oncogenic activity since both the catalytic domain and scaffold function are essential for SFKs (10). The myristoyl group may participate in protein folding and promote Src kinase to switch to its active conformation leading to phosphorylation at Tyr416 (25). Loss of myristoylation suppresses down-stream signaling including FAK as well as the MAPK signaling pathway (13). Additionally, inhibition of myristoylation blocks the scaffold function of Src kinase, and prevents the protein–protein interaction with AR thus inhibiting androgen independent AR activation. Several studies have reported that high levels of Src kinase dead mutants are still able to enhance FAK catalytic activity (26) and decrease osteoporosis in the $Src^{-/-}$ animal model (27), and promote AR activity in part (12). Inhibition of Src kinase anchoring to the intracellular membrane could change the protein intracellular trafficking path (23). Inhibition of NMT provides an additional pathway to inhibit SFK-mediated oncogenic signaling in comparison with numerous Src kinase inhibitors such as dasatinib that only target the ATP binding site (28). We show that expression of NMT1 is correlated with expression levels of Src kinase in human tumors. Given the fact that the elevation of Src expression and activity has been well documented in advanced prostate cancer (9), targeting the NMT1-Src axis provides a novel approach for inhibiting tumor progression, particularly in Src-driven tumors.

Although numerous NMT inhibitors have been developed as antiviral, antifungal or antiparastic agents (29), only a limited number of inhibitors including COPP24 and “Compound 1” have been reported as anticancer agents (30, 31). NMT activity occurs via the formation of a ternary complex with myristoyl-CoA and glycine at the N-terminus of the target proteins (32). Our study identifies B13 as a novel NMT inhibitor that can be modeled into the myristoyl-CoA binding site in NMT. B13 shows limited effect on normal cells or organs, which may be due to elevated fatty acid metabolism and lipogenesis in cancer cells in comparison with normal cells (33). Elevated expression of fatty acid synthase (FASN) has been well documented in numerous cancers, and targeting FASN shows benefit in inhibiting cancer progression (34). Biosynthesis of acyl-CoAs including myristoyl-CoA is a required step for phospholipid synthesis (35). In concert with aberrant expression of NMT in a variety of cancer cells (3, 21, 36), an increase of myristoyl-CoA production either from exogenous fatty acids or through *de novo* synthesis could further promote protein myristoylation to facilitate the growth of cancer cells (35). In particular, Src expression and/or activity are highly elevated in advanced prostate cancer (9). Further studies are required to determine if the amount of myristoylated Src, which is essential for its kinase activity, is also elevated in advanced prostate cancer. Nevertheless, the differential activity of fatty acid metabolism coupled with an elevation of NMT enzymatic activity might provide a molecular basis to differentiate cancer cells with normal cells. Our study emphasizes the NMT1-Src axis in mediation of the growth of prostate cancer cells. It should be noted that

targeting NMT may also lead to inhibition of other NMT downstream proteins in which myristoylation is essential for their function. For example, myristoylation of AMPK is required for its recruitment to the mitochondria for the induction of mitophagy and cell viability (37). The inhibition of B13 on NMT1 activity could potentially block the AMPK recruitment process to inhibit the proliferation of prostate cancer cells. Regardless, our study has demonstrated that targeting NMT activity provides a promising therapeutic approach for treatment of cancer progression.

It should be noted that B13 could have other inhibitory targets in addition to NMT1. For example, it has been reported that B13 can inhibit acid ceramidase (38, 39). The inhibition suppresses the conversion of ceramide to sphingosine, which leads to an increase of ceramide levels including C_{14}-, C_{16}-, C_{24}-, $C_{24:1}$-ceramides and a decrease of sphingosine (24, 38, 39). The alteration of ceramides and sphingosine triggers the cell apoptosis pathway (40). It remains to be studied if inhibition of NMT activity could also contribute to the alteration of ceramide levels. The biosynthesis of ceramides requires fatty acyl-CoA as substrates, and the accumulation of myristoyl-CoA resulting from the blockade of NMT activity might potentially facilitate ceramide biosynthesis. Therefore, B13 might potentially be a dual inhibitor in targeting both NMT and acid ceramidase.

Further optimization of B13 and development of a drug delivery vehicle may improve the efficacy for cancer treatment. We have illustrated that LCL204, a B13 derivative identified by structure replacement, shows 9-fold decrease in IC_{50} on NMT1 enzymatic activity. Interestingly, LCL204 is also reported as an inhibitor of acid ceramidase with higher inhibitory potential than B13 (38). Further development of LCL204 will rely on its toxicity to normal cells and organs in pre-clinical trials. Additionally, the myristoyl group of B13 confers hydrophobicity to the compound. Using a nanoparticle-based vehicle to deliver the compound might be helpful for the improvement of its efficacy *in vivo* and reduction of adverse side effects in cancer treatment (41).

Supplementary Material

Refer to Web version on PubMed Central for supplementary material.

Acknowledgments

Financial Support: This work was supported by NIH (R01CA172495) and DOD (W81XWH-15-1-0507) to H. Cai, and P30 CA138313 to A. Bielawska.

References

1. Bhatnagar RS, Futterer K, Farazi TA, Korolev S, Murray CL, Jackson-Machelski E, et al. Structure of N-myristoyltransferase with bound myristoylCoA and peptide substrate analogs. Nat Struct Biol. 1998; 5:1091–7. [PubMed: 9846880]
2. Yang SH, Shrivastav A, Kosinski C, Sharma RK, Chen MH, Berthiaume LG, et al. N-myristoyltransferase 1 is essential in early mouse development. The Journal of biological chemistry. 2005; 280:18990–5. [PubMed: 15753093]
3. Felsted RL, Glover CJ, Hartman K. Protein N-myristoylation as a chemotherapeutic target for cancer. J Natl Cancer Inst. 1995; 87:1571–3. [PubMed: 7563194]

4. Resh MD. Myristylation and palmitylation of Src family members: the fats of the matter. Cell. 1994; 76:411–3.
5. Patwardhan P, Resh MD. Myristoylation and membrane binding regulate c-Src stability and kinase activity. Molecular and cellular biology. 2010; 30:4094–107. [PubMed: 20584982]
6. Summy JM, Gallick GE. Treatment for advanced tumors: SRC reclaims center stage. Clin Cancer Res. 2006; 12:1398–401. [PubMed: 16533761]
7. Gioeli D. Signal transduction in prostate cancer progression. Clinical science. 2005; 108:293–308. [PubMed: 15603554]
8. Blume-Jensen P, Hunter T. Oncogenic kinase signalling. Nature. 2001; 411:355–65. [PubMed: 11357143]
9. Guo Z, Dai B, Jiang T, Xu K, Xie Y, Kim O, et al. Regulation of androgen receptor activity by tyrosine phosphorylation. Cancer Cell. 2006; 10:309–19. [PubMed: 17045208]
10. Thomas SM, Brugge JS. Cellular functions regulated by Src family kinases. Annu Rev Cell Dev Biol. 1997; 13:513–609. [PubMed: 9442882]
11. Chen Y, Sawyers CL, Scher HI. Targeting the androgen receptor pathway in prostate cancer. Curr Opin Pharmacol. 2008; 8:440–8. [PubMed: 18674639]
12. Cai H, Babic I, Wei X, Huang J, Witte ON. Invasive Prostate Carcinoma Driven by c-Src and Androgen Receptor Synergy. Cancer Res. 2011; 71:862–72. [PubMed: 21135112]
13. Ducker CE, Upson JJ, French KJ, Smith CD. Two N-myristoyltransferase isozymes play unique roles in protein myristoylation, proliferation, and apoptosis. Mol Cancer Res. 2005; 3:463–76. [PubMed: 16123142]
14. Xin L, Teitell MA, Lawson DA, Kwon A, Mellinghoff IK, Witte ON. Progression of prostate cancer by synergy of AKT with genotropic and nongenotropic actions of the androgen receptor. Proc Natl Acad Sci U S A. 2006; 103:7789–94. [PubMed: 16682621]
15. Cai H, Smith DA, Memarzadeh S, Lowell CA, Cooper JA, Witte ON. Differential transformation capacity of Src family kinases during the initiation of prostate cancer. Proceedings of the National Academy of Sciences of the United States of America. 2011; 108:6579–84. [PubMed: 21464326]
16. Haack K, Cockrell AS, Ma H, Israeli D, Ho SN, McCown TJ, et al. Transactivator and structurally optimized inducible lentiviral vectors. Molecular therapy : the journal of the American Society of Gene Therapy. 2004; 10:585–96. [PubMed: 15336658]
17. Cai H, Smith DA, Memarzadeh S, Lowell CA, Cooper JA, Witte ON. Differential transformation capacity of Src family kinases during the initiation of prostate cancer. Proceedings of the National Academy of Sciences of the United States of America. 2011; 108:6579–84. [PubMed: 21464326]
18. Sunkel B, Wu D, Chen Z, Wang CM, Liu X, Ye Z, et al. Integrative analysis identifies targetable CREB1/FoxA1 transcriptional co-regulation as a predictor of prostate cancer recurrence. Nucleic acids research. 2016; 44:4105–22. [PubMed: 26743006]
19. Adam RM, Yang W, Di Vizio D, Mukhopadhyay NK, Steen H. Rapid preparation of nuclei-depleted detergent-resistant membrane fractions suitable for proteomics analysis. BMC Cell Biol. 2008; 9:30. [PubMed: 18534013]
20. Thinon E, Serwa RA, Broncel M, Brannigan JA, Brassat U, Wright MH, et al. Global profiling of co- and post-translationally N-myristoylated proteomes in human cells. Nat Commun. 2014; 5:4919. [PubMed: 25255805]
21. Wright MH, Heal WP, Mann DJ, Tate EW. Protein myristoylation in health and disease. J Chem Biol. 2010; 3:19–35. [PubMed: 19898886]
22. Aleshin A, Finn RS. SRC: a century of science brought to the clinic. Neoplasia. 2010; 12:599–607. [PubMed: 20689754]
23. Sato I, Obata Y, Kasahara K, Nakayama Y, Fukumoto Y, Yamasaki T, et al. Differential trafficking of Src, Lyn, Yes and Fyn is specified by the state of palmitoylation in the SH4 domain. Journal of cell science. 2009; 122:965–75. [PubMed: 19258394]
24. Szulc ZM, Mayroo N, Bai A, Bielawski J, Liu X, Norris JS, et al. Novel analogs of D-e-MAPP and B13. Part 1: synthesis and evaluation as potential anticancer agents. Bioorganic & medicinal chemistry. 2008; 16:1015–31. [PubMed: 17869115]
25. Bagrodia S, Taylor SJ, Shalloway D. Myristylation is required for Tyr-527 dephosphorylation and activation of pp60c-src in mitosis. Mol Cell Biol. 1993; 13:1464–70. [PubMed: 7680096]

26. Cary LA, Klinghoffer RA, Sachsenmaier C, Cooper JA. SRC catalytic but not scaffolding function is needed for integrin-regulated tyrosine phosphorylation, cell migration, and cell spreading. Mol Cell Biol. 2002; 22:2427–40. [PubMed: 11909938]
27. Schwartzberg PL, Xing L, Hoffmann O, Lowell CA, Garrett L, Boyce BF, et al. Rescue of osteoclast function by transgenic expression of kinase-deficient Src in src−/− mutant mice. Genes Dev. 1997; 11:2835–44. [PubMed: 9353253]
28. Araujo JC, Trudel GC, Saad F, Armstrong AJ, Yu EY, Bellmunt J, et al. Docetaxel and dasatinib or placebo in men with metastatic castration-resistant prostate cancer (READY): a randomised, double-blind phase 3 trial. The lancet oncology. 2013; 14:1307–16. [PubMed: 24211163]
29. Zhao C, Ma S. Recent advances in the discovery of N-myristoyltransferase inhibitors. ChemMedChem. 2014; 9:2425–37. [PubMed: 25125080]
30. French KJ, Zhuang Y, Schrecengost RS, Copper JE, Xia Z, Smith CD. Cyclohexyl-octahydro-pyrrolo[1,2-a]pyrazine-based inhibitors of human N-myristoyltransferase-1. J Pharmacol Exp Ther. 2004; 309:340–7. [PubMed: 14724220]
31. Thinon E, Morales-Sanfrutos J, Mann DJ, Tate EW. N-Myristoyltransferase Inhibition Induces ER-Stress, Cell Cycle Arrest, and Apoptosis in Cancer Cells. ACS chemical biology. 2016; 11:2165–76. [PubMed: 27267252]
32. Farazi TA, Waksman G, Gordon JI. The biology and enzymology of protein N-myristoylation. J Biol Chem. 2001; 276:39501–4. [PubMed: 11527981]
33. Menendez JA, Lupu R. Fatty acid synthase and the lipogenic phenotype in cancer pathogenesis. Nat Rev Cancer. 2007; 7:763–77. [PubMed: 17882277]
34. Sounni NE, Cimino J, Blacher S, Primac I, Truong A, Mazzucchelli G, et al. Blocking lipid synthesis overcomes tumor regrowth and metastasis after antiangiogenic therapy withdrawal. Cell Metab. 2014; 20:280–94. [PubMed: 25017943]
35. Grevengoed TJ, Klett EL, Coleman RA. Acyl-CoA metabolism and partitioning. Annu Rev Nutr. 2014; 34:1–30. [PubMed: 24819326]
36. Rajala RV, Radhi JM, Kakkar R, Datla RS, Sharma RK. Increased expression of N-myristoyltransferase in gallbladder carcinomas. Cancer. 2000; 88:1992–9. [PubMed: 10813869]
37. Liang J, Xu ZX, Ding Z, Lu Y, Yu Q, Werle KD, et al. Myristoylation confers noncanonical AMPK functions in autophagy selectivity and mitochondrial surveillance. Nature communications. 2015; 6:7926.
38. Bielawska A, Bielawski J, Szulc ZM, Mayroo N, Liu X, Bai A, et al. Novel analogs of D-e-MAPP and B13. Part 2: signature effects on bioactive sphingolipids. Bioorganic & medicinal chemistry. 2008; 16:1032–45. [PubMed: 17881234]
39. Samsel L, Zaidel G, Drumgoole HM, Jelovac D, Drachenberg C, Rhee JG, et al. The ceramide analog, B13, induces apoptosis in prostate cancer cell lines and inhibits tumor growth in prostate cancer xenografts. Prostate. 2004; 58:382–93. [PubMed: 14968439]
40. Ogretmen B, Hannun YA. Biologically active sphingolipids in cancer pathogenesis and treatment. Nat Rev Cancer. 2004; 4:604–16. [PubMed: 15286740]
41. Nagesh PK, Johnson NR, Boya VK, Chowdhury P, Othman SF, Khalilzad-Sharghi V, et al. PSMA targeted docetaxel-loaded superparamagnetic iron oxide nanoparticles for prostate cancer. Colloids Surf B Biointerfaces. 2016; 144:8–20. [PubMed: 27058278]

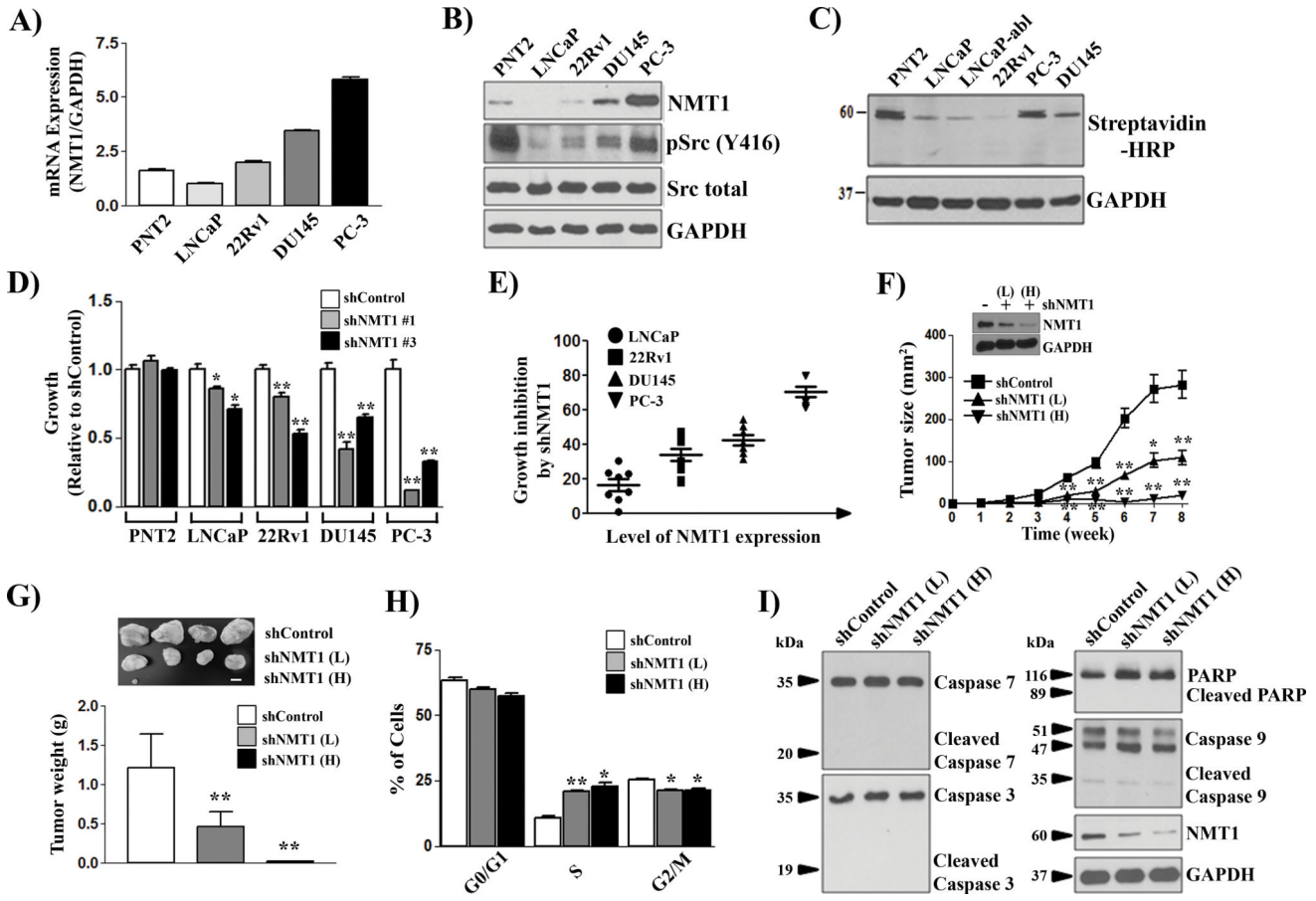

Figure 1. NMT1 regulates the proliferation of prostate cancer cells and xenograft tumors

(A–C) PNT2 (normal prostate cells) and prostate cancer cells were grown with 60 μM myristic acid-azide. Cell lysates were subjected to Click chemistry for detecting myristoylated proteins. Expression levels of NMT1 mRNA (A), protein (B), and myristoylated proteins (C) were analyzed. Note: PNT2 cells are immortalized by the large T-antigen, which usually leads to the activation of Src kinase. **(D)** NMT1 was knocked down by two independent shRNA-NMT1 by lentiviral infection and proliferation measured after 5 d. Data are relative to the control (set as 1). Also see Supplemental Figure S1 for the growth curve. **(E)** The correlation of NMT1 expression levels with growth inhibitory rate of shRNA-NMT1. **(F–G)** PC-3 cancer cells infected with control shRNA or shRNA-NMT1 of low titer (L, MOI=10) and high titer (H, MOI=50) were implanted subcutaneously in SCID mice (n=6 per group). Tumor size was measured weekly and tumor weight measured at week 8. **(H–I)** PC-3 cancer cells infected with control shRNA or shRNA-NMT1 (L, MOI=10; H, MOI=50) were cultured for 3 d followed by cell cycle analysis. The percentage of the cells in G0/G1, S, and G2/M phases is relative to the control shRNA (H). Levels of the indicated apoptosis-related proteins were detected by immunoblotting (I). *: $p<0.05$; **: $p<0.01$.

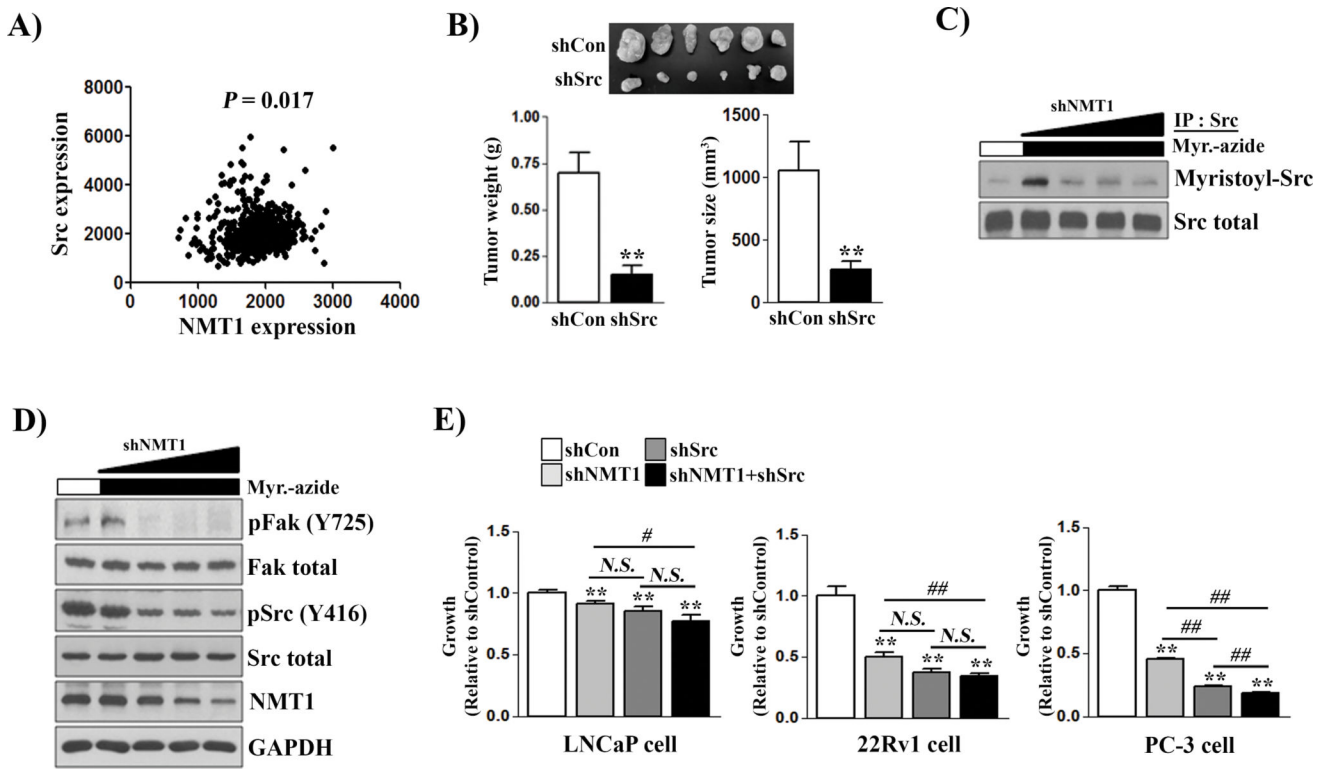

Figure 2. NMT1 knockdown causes tumor suppression by down-regulation of Src kinase myristoylation and tyrosine phosphorylation

(A) Correlation of Src and NMT1 expression (copy number from the TCGA database (n = 498 tumors). **(B)** PC-3 cancer cells infected with control shRNA or shRNA-Src were implanted subcutaneously in SCID mice (n=6 per group). The size and weight of xenograft tumors were measured at week 8. **(C–D)** PC-3 cancer cells were transduced with shRNA-NMT1 (MOI= 0, 10, 30, 50) by lentiviral infection. The transduced cells were grown with/without myristic acid-azide and myristoylated Src was detected by Click chemistry and immunoblotting with streptavidin-HRP **(C)**. The expression levels of the indicated proteins from the protein lysates were measured by immunoblotting (D). **(E)** LNCaP, 22Rv1, and PC-3 cancer cells were transduced with control, shRNA-NMT1, shRNA-Src, or both and proliferation was measured by the MTT assay after 5 d. Data are relative to the control (set as 1). **: $p<0.01$ (each treatment group was compared with the control group). #: $p<0.05$; ##: $p<0.01$ (the compared groups were indicated in the figure).

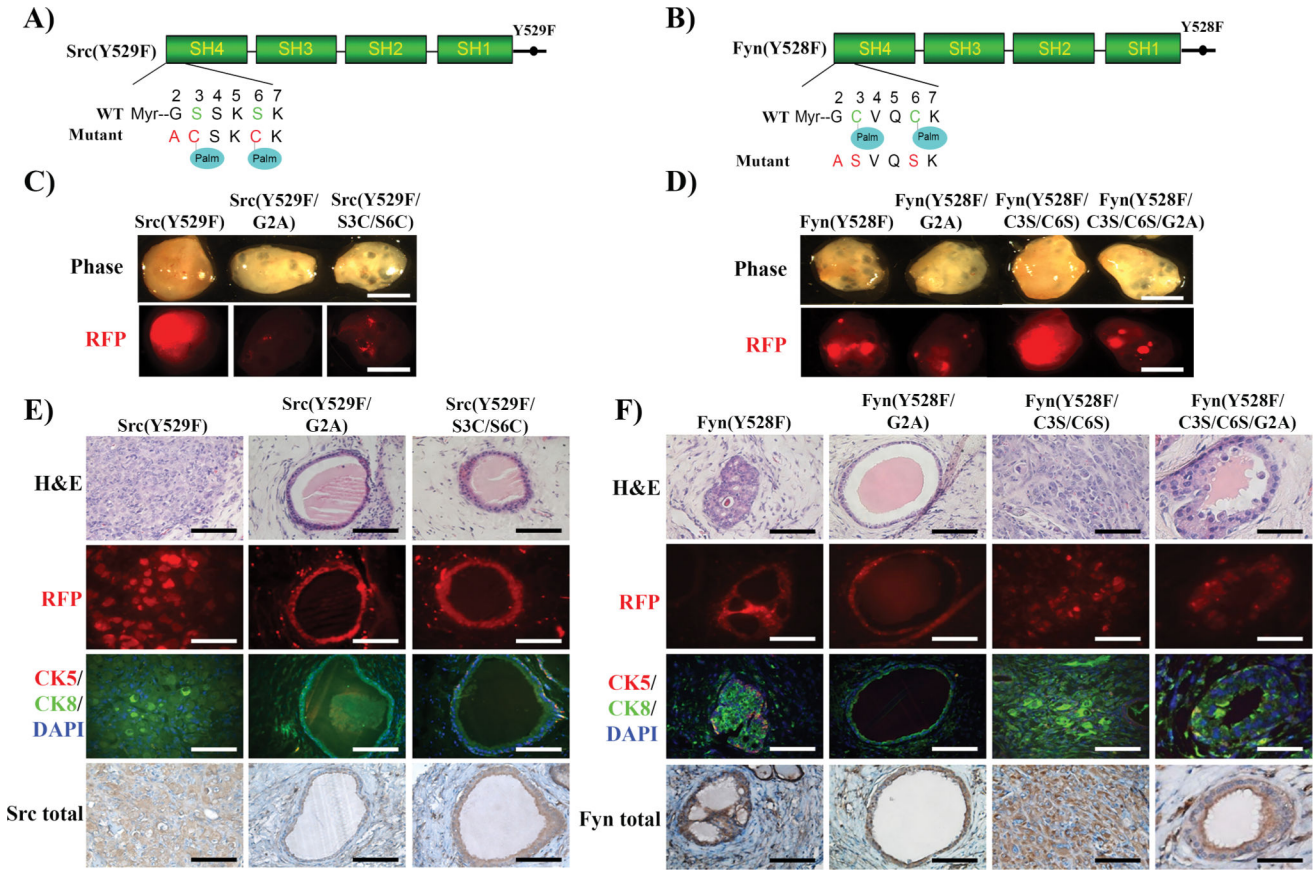

Figure 3. Loss of myristoylation inhibits SFK mediated tumorigenesis

(A–B) Schematic of constitutively active Src(Y529F) and Fyn(Y528F) mutations resulting in loss of myristoylation and gain or loss of palmitoylation sites. Gly2 was mutated to Ala (loss of myristoylation site) in constitutively active Src(Y529F) or Fyn(Y528F) kinases. Ser3 and Ser6 sites of Src(Y529F) were mutated to Cys (gain of palmitoylation sites), and the Cys3 and Cys6 sites of Fyn(Y528F) were mutated to Ser (loss of palmitoylation sites). **(C-D)** The *in vivo* prostate regeneration assay was performed with the Src(Y529F) or Fyn(Y528F) and acylation mutants (RFP marker). Representative images of regenerated prostate tissue and RFP detection. Scale bar, 2 mm. **(E–F)** Representative H&E, RFP fluorescence, and IHC staining of CK5 (basal mark, red)/CK8(luminal mark, green)/DAPI (nucleus staining), and Src kinase or Fyn kinase in the regenerated tissues. Scale bar, 100 μm.

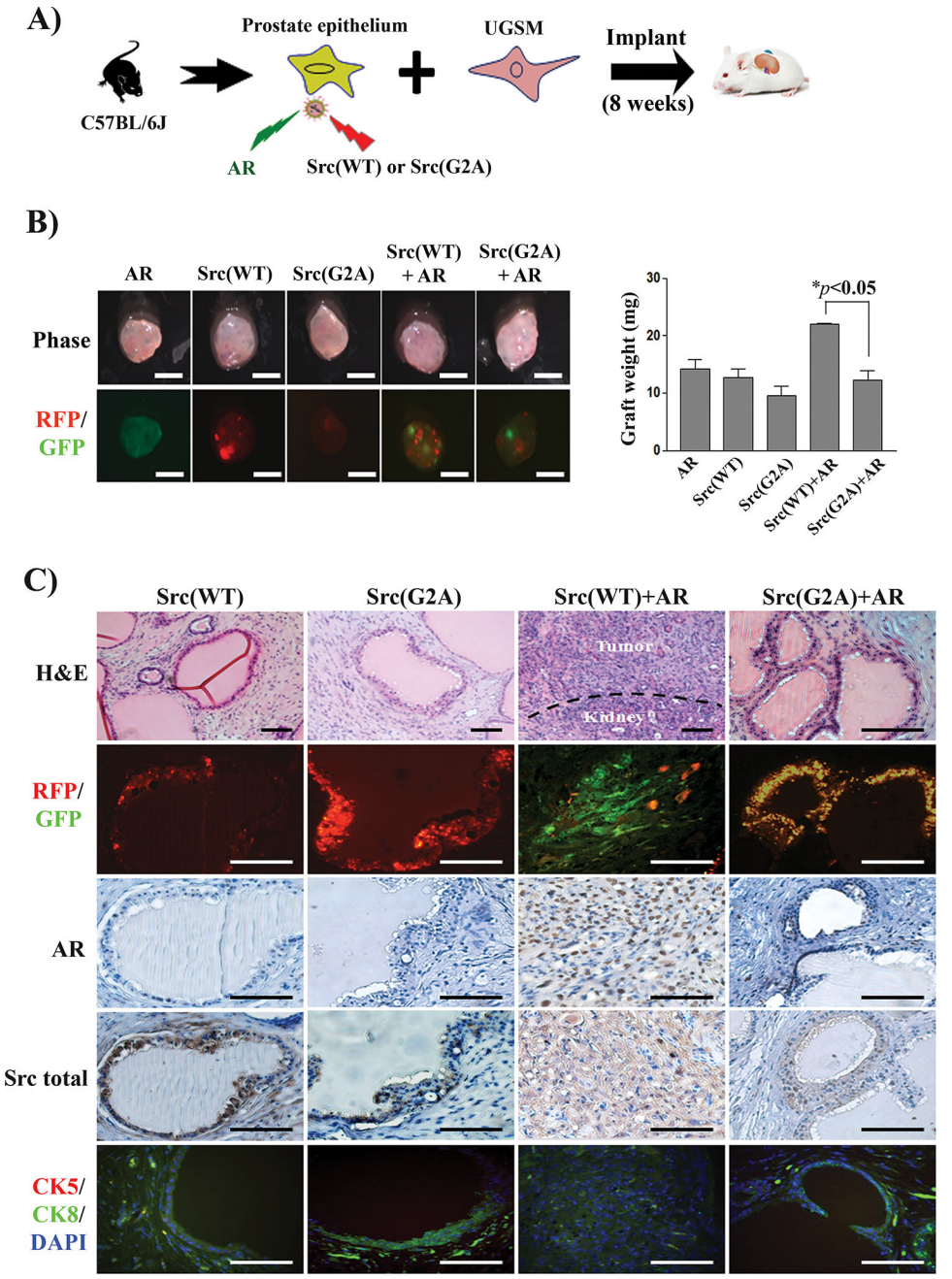

Figure 4. Loss of myristoylation in Src kinase inhibits the synergy of Src(WT) with androgen receptor (AR) in prostate tumorigenesis

(A) Schematic for examining the synergy of Src and AR in prostate tumorigenesis. Primary prostate epithelial cells were transduced with AR (GFP marker), Src(WT) (RFP marker), Src(G2A) (RFP marker), or co-transduced with Src(WT)/Src(G2A) and AR and the infected cells were combined with UGSM, and implanted under the renal capsule of SCID mice. Regenerated prostate tissue was isolated after 8 weeks. **(B)** Representative images of regenerated prostate tissue and RFP/GFP detection (scale bar, 2 mm). The weight of prostate tissues was compared in the bar graph. The * indicates an unpaired, two-tailed t test. **(C)**

H&E, RFP/GFP, and IHC staining of AR and total Src, and co-staining of CK8, CK5 and DAPI in regenerated tissue. Scale bar, 100 μm.

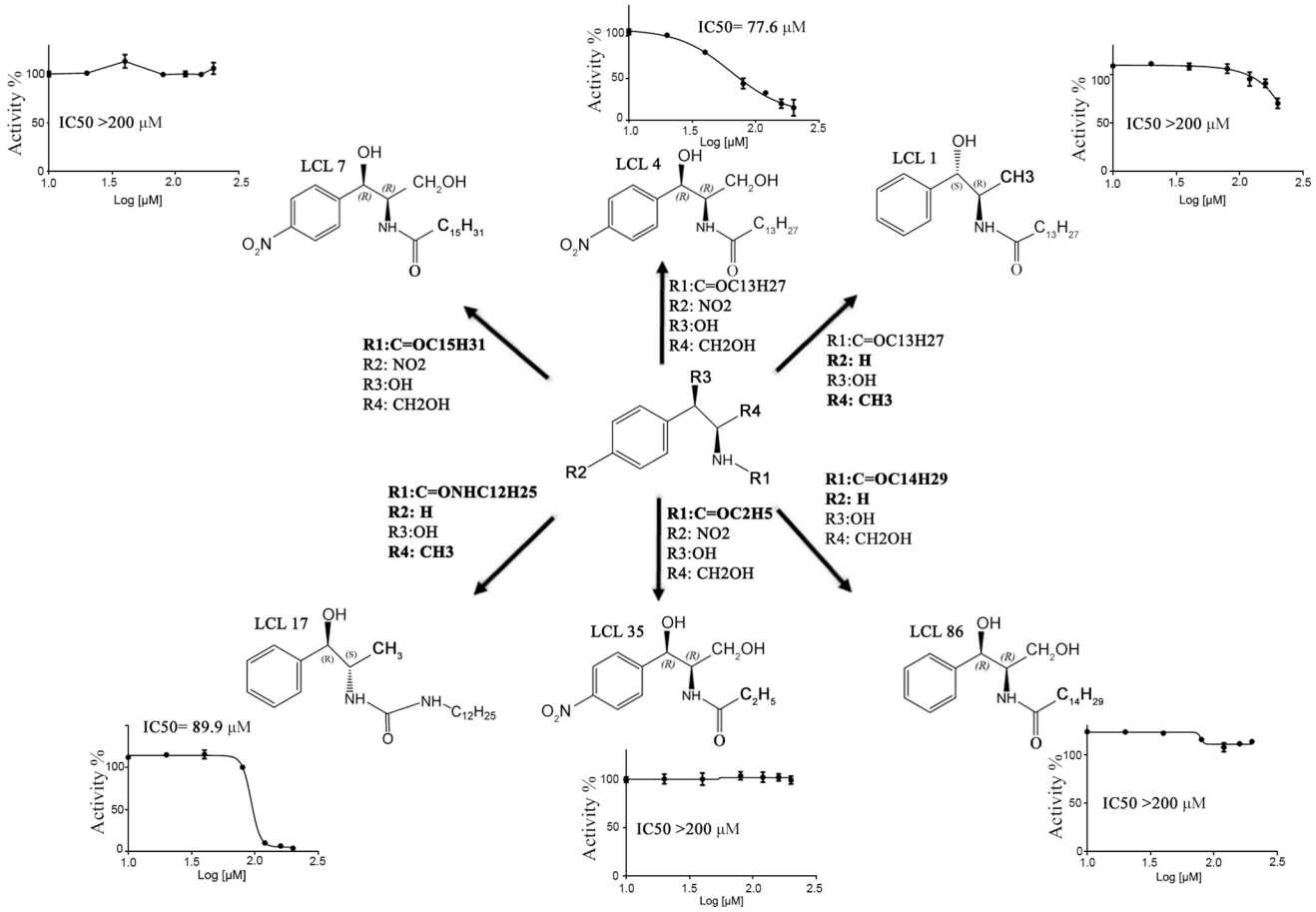

Figure 5. Chemical structures and IC_{50} values of LCL compounds targeting NMT1 enzymatic activity

The IC_{50} of LCL compounds on NMT1 enzymatic activity was measured. LCL7 and LCL35 represent a compound with a longer and shorter acyl-chain (R1 group in Figure 5A) than LCL4/B13, respectively. LCL17 represents a compound with NH group in the acyl-chain, which enhances inhibitory effect. LCL86 represents a compound with longer acyl-chain and without nitro group (R2 group). LCL1 represents a compound without both nitro and hydroxyl group (R4 group). The bold highlights the chemical groups different to LCL4/B13 compound.

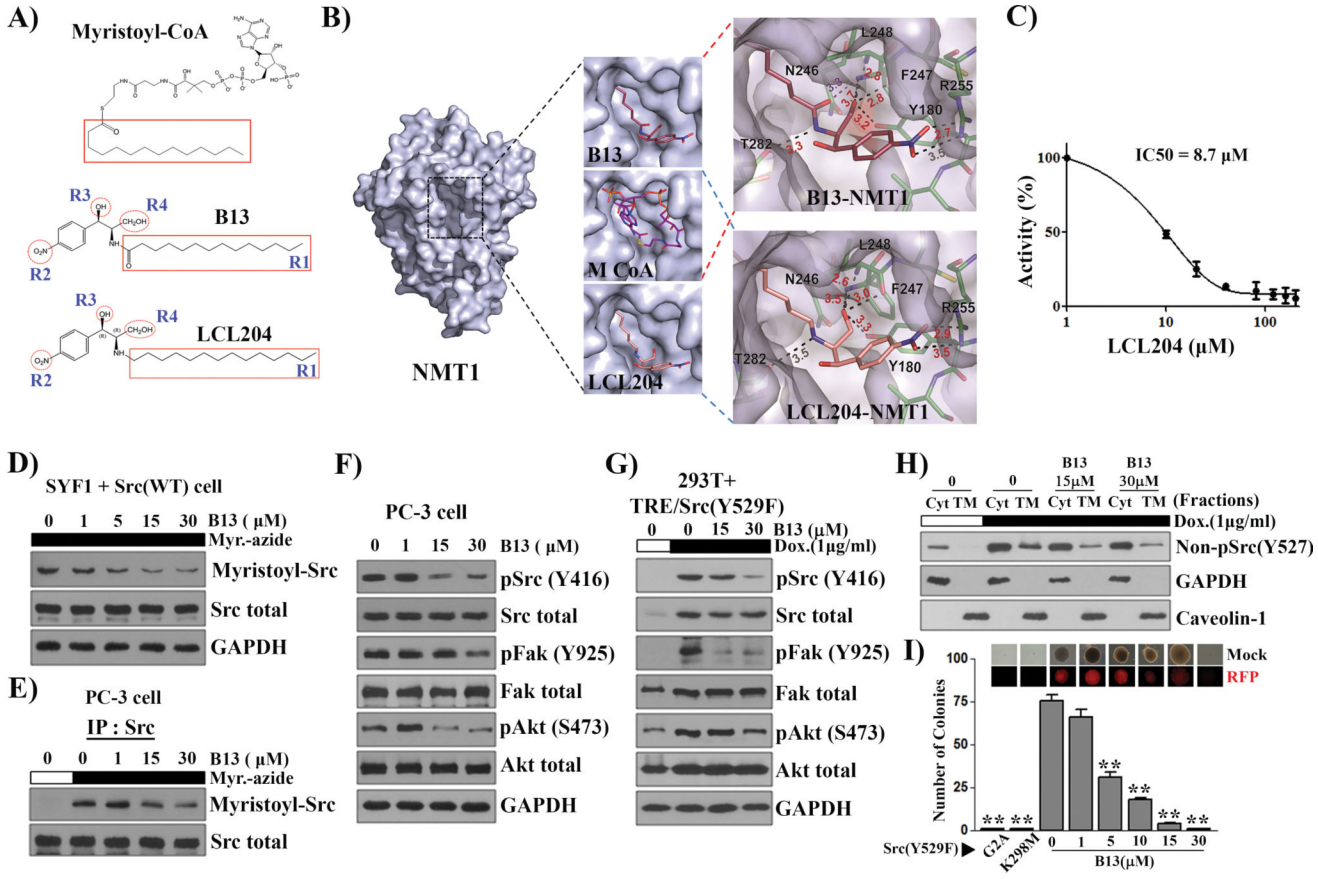

Figure 6. Myristoyl-CoA analog, B13, inhibits NMT1 enzymatic activity and suppresses Src kinase mediated cell transformation

(A) Comparison of the myristoyl-CoA structure with B13 and LCL204. The C14 acyl-group (R1) highlighted with a red square in B13 is identical with that in myristoyl-CoA. R2 (nitro group), R3 (hydroxyl group), and R4 (hydroxymethyl group) are important for the inhibitory effect based on structure-activity relationship (SAR) analysis in the Supplemental Figure S9. **(B)** The analysis of the NMT1 protein structure with B13 and LCL204 inhibitor. The binding site of myristoyl-CoA with the NMT1 crystal structure was replaced with B13. The upper right panel shows B13 interactions with neighboring side chains. Myristoyl-CoA and LCL204 were modeled in the NMT1 binding pocket. The bottom right panel shows that LCL204 interactions with the neighboring side chains. According to the structure replacement, the replacement of the methoxide group in B13 with $-CH_2$ led to a B13 derivative, LCL204, which favors the interactions of the functional groups with amino acids in the binding pocket of NMT1. **(C)** The inhibitory effect of LCL204 on NMT1 enzymatic activity. The IC_{50} of LCL204 on NMT1 enzymatic activity was 8.7 μM, which increased about 9-fold in comparison with that of B13. **(D–E)** SYF1 cells were transduced with Src(WT) and the transduced cells, SYF1+Src(WT) (D) or PC-3, (E) were cultured with B13 overnight followed by myristic acid-azide (60 μM) for 8 h. The lysates from SYF1+Src(WT) cells (D) and Src immunoprecipitates from PC-3 cells (E) were subjected to Click chemistry. The expression levels of myristoyl-Src detected by streptavidin-HRP, total Src, and GAPDH were analyzed by immunoblotting. **(F)** The expression levels of the indicated proteins in the

total lysates from (E) were measured by immunoblotting. **(G)** 293T cells expressing doxycycline inducible Src(Y529F) were treated with/without doxycycline (Dox, 1μg/ml) and with 0 (DMSO), 15, and 30 μM of B13 for 24 h. The levels of the indicated proteins were determined by immunoblotting. **(H)** The lysate from (G) was fractionated. Caveolin-1 and GAPDH were used as markers for total cytoplasmic membrane (TM) and cytosolic fraction (Cyt), respectively. Immunoblot detection using the non-pSrc(Y527F) antibody represented the *de novo* synthesized Src kinase. **(I)** SYF1 cells were transduced with Src (Y529F), Src (Y529F/G2A), or Src (Y529F/K298M) and subjected to the soft agar assay. SYF1-Src(Y529F) cells were treated with B13 and the number of resulting colonies was counted. Representative phase and RFP images of colonies in the soft agar assay are displayed. **: $P<0.01$.

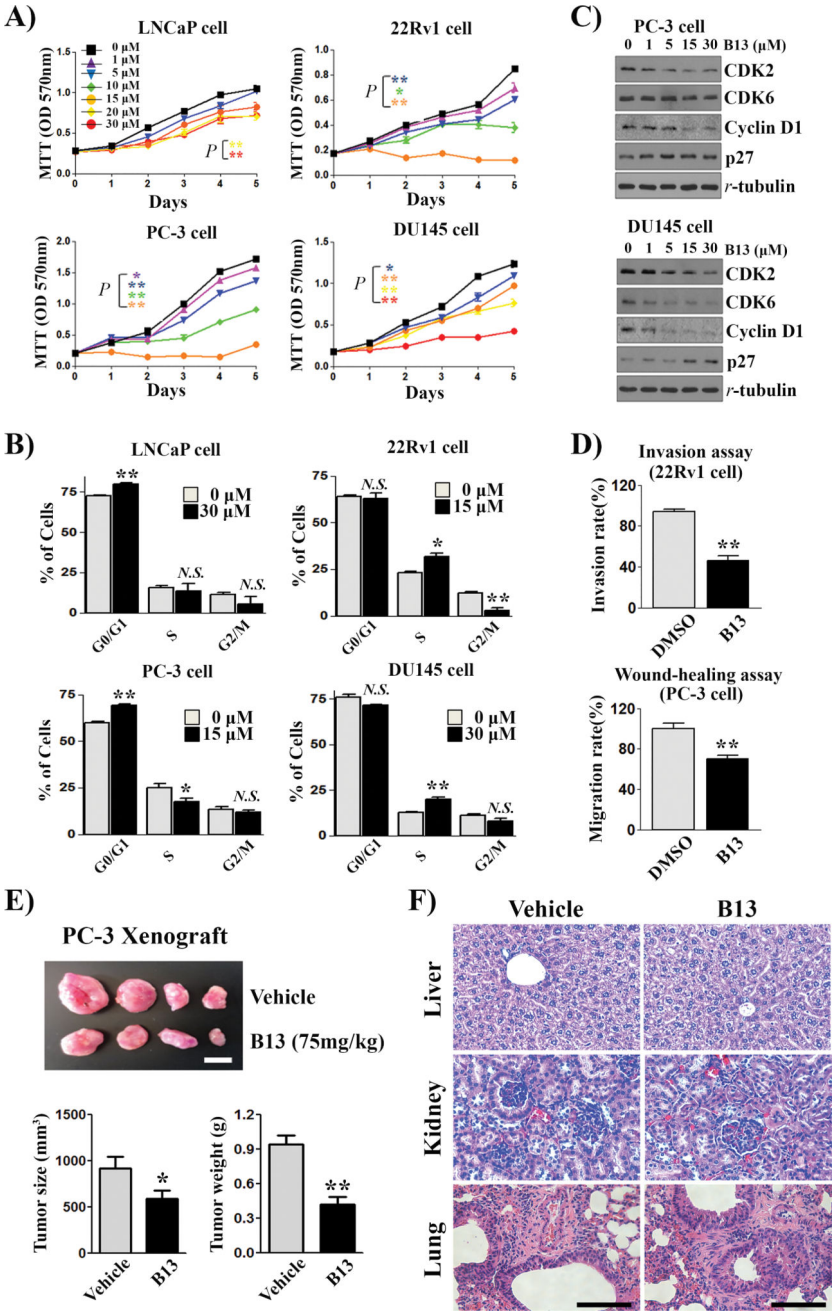

Figure 7. The myristoyl-CoA analog B13 inhibits cell cycle progression and growth of xenograft tumors

(A) Prostate cancer cell lines were cultured with B13 for 5 d and cell proliferation was measured. The value is expressed as the mean ± SEM (n=6 wells). The statistical analysis is indicated by the color representing the labeled concentration of B13 treatment. **(B)** Cell cycle analysis of LNCaP, 22Rv1, PC-3, and DU145 cells cultured with B13 for 3 d. The percentage of cells in G0/G1, S, and G2/M phases was compared between the control and B13 treatment. **(C)** PC-3 and DU-145 cells treated with/without different concentrations of B13 were analyzed for the expression levels of CDK2, CDK6, cyclin D1, p27, and tubulin

by immunoblotting. **(D)** 22Rv1 and PC-3 cancer cells grown with/without 15 μM B13 were examined in the Transwell invasion assay and the wound-healing assay, respectively. **(E)** PC-3 prostate cancer cells were subcutaneously injected into both flank sides of SCID mice (3 months-old, n=6 per group). Vehicle or B13 (75mg/kg/mouse) were administered intravenously twice a week for 6 weeks. Representative images of the xenograft tumors are shown (upper panel; scale bar, 10 mm). The size and weight of xenograft tumors were measured as mean ± SEM (bottom panel). *: $P<0.05$, **: $P<0.01$. **(F)** Histology analysis of B13 on major organs. H&E staining of liver, kidney, and lung tissues derived from (E) were evaluated. Scale bar, 400 μm.